LETTERS
PUBLISHED ONLINE: 16 SEPTEMBER 2012 | DOI: 10.1038/NMAT3415
nature materials

A ferroelectric memristor

André Chanthbouala[1], Vincent Garcia[1], Ryan O. Cherifi[1], Karim Bouzehouane[1], Stéphane Fusil[1,2], Xavier Moya[3], Stéphane Xavier[4], Hiroyuki Yamada[1,5], Cyrile Deranlot[1], Neil D. Mathur[3], Manuel Bibes[1], Agnès Barthélémy[1]* and Julie Grollier[1]

Memristors are continuously tunable resistors that emulate biological synapses[1,2]. Conceptualized in the 1970s, they traditionally operate by voltage-induced displacements of matter, although the details of the mechanism remain under debate[3–5]. Purely electronic memristors based on well-established physical phenomena with albeit modest resistance changes have also emerged[6,7]. Here we demonstrate that voltage-controlled domain configurations in ferroelectric tunnel barriers[8–10] yield memristive behaviour with resistance variations exceeding two orders of magnitude and a 10 ns operation speed. Using models of ferroelectric-domain nucleation and growth[11,12], we explain the quasi-continuous resistance variations and derive a simple analytical expression for the memristive effect. Our results suggest new opportunities for ferroelectrics as the hardware basis of future neuromorphic computational architectures.

In tunnel junctions with a ferroelectric barrier, switching the ferroelectric polarization induces variations of the tunnel resistance, with resistance contrasts between the ON and OFF states of several orders of magnitude[9,13–15], defining a giant tunnel electroresistance effect. Several mechanisms have been proposed to explain this behaviour[16–18] but the dominant one seems related to changes in the tunnel barrier potential profile due to asymmetric polarization screening at barrier/electrode interfaces. In analogy with the operation of ferroelectric random access memories, the large OFF/ON ratio in ferroelectric tunnel junctions (FTJs) has so far been considered only for binary data storage, with the key advantage of non-destructive readout and simpler device architecture. An important degree of freedom that has not yet been exploited in FTJs is the domain structure of the ferroelectric tunnel barrier. In ferroelectrics the domain size scales down with the square root of the film thickness[19,20], so that nanometre-size domains are expected for ferroelectric tunnel barriers (which are typically thinner than 5 nm). This provides a very fine level of control for the relative proportion of up and down domains and thereby of properties depending on the switched polarization[21].

Here we show that the domain configuration of a ferroelectric tunnel barrier can be controllably used to produce a virtually continuous range of resistance levels between OFF and ON states. We report piezoresponse force microscopy (PFM) images and electrical transport measurements as a function of the amplitude, duration and repetition number of voltage pulses in the 10–200 ns range. In a simple picture of conduction in parallel by up and down domains, we argue that the resistance variations are ruled by ferroelectric domain dynamics during polarization reversal. We analyse both OFF to ON and ON to OFF switching processes and model them in terms of domain nucleation and propagation. We conclude that FTJs emerge as a new class of memristive systems for which state equations can be derived from models of polarization dynamics.

Our FTJs are composed of $BaTiO_3$(2 nm)/$La_{0.67}Sr_{0.33}MnO_3$ (30 nm) (BTO/LSMO) extended layers on which Co/Au pads are defined by electron beam lithography (typical diameter 350 nm), sputtering and lift-off. Details of the growth and fabrication methods, as well as a demonstration of the ferroelectric properties of the BTO barrier have been given elsewhere[9,14]. Electrical contact to the pads was made using the conductive tip of an atomic force microscope. The measurements are performed by applying short (t_{pulse} = 10–200 ns) write voltage pulses (of amplitude V_{write}) between the tip and the bottom electrode and subsequently measuring the tunnel resistance at low d.c. voltage ($|V_{read}| = 100$ mV).

Figure 1a shows a plot of the junction resistance as we vary the amplitude of the applied voltage pulses while keeping a fixed pulse duration of 20 ns. A hysteretic cycle between low ($R_{ON} \sim 1.6 \times 10^5\ \Omega$) and high ($R_{OFF} \sim 4.6 \times 10^7\ \Omega$) resistance states is observed, with a large OFF/ON ratio of ~300 when the write voltage is swept between −5.6 and +4.2 V (Fig. 1a, blue curve). Following previous results[14], the low-resistance state (R_{ON}) corresponds to the ferroelectric polarization pointing up ($P_\uparrow$), that is, towards the Co/Au pad, which is also the virgin state for all devices. The switching between the two states is bipolar and, interestingly, not abrupt; that is, a broad range of intermediate resistance states are observed. An asymmetry in the switching is visible and may reflect the presence of downward-polarized interfacial dipoles that favour the initial growth of downward polarized domains[22]. The minor loops in Fig. 1a (cyan to red curves) show that depending on the cycling protocol the final resistance state can be finely tuned between R_{ON} and R_{OFF}.

To gain insight into the microscopic mechanisms responsible for this memristive effect, we investigate the correspondence between the resistance value and the ferroelectric domain configuration. We have collected PFM images after poling the junctions into different resistance states (see Fig. 1b). Starting from a virtually homogeneous up-polarized state corresponding to a low-resistance value ($R = 3 \times 10^5\ \Omega$, that is close to the ON state), the application of positive voltage pulses nucleates down-polarized domains (white contrast in the red-framed images). Applying consecutive pulses of increasing amplitude causes the expansion of these existing down-polarized domains as well as the nucleation of new ones, consistent with previous results on thick ferroelectric films[23,24]. An almost saturated down state ($R = 2 \times 10^7\ \Omega$, that is, close to the OFF state) is eventually reached. In the opposite case, applying negative pulses leads to a decrease in the resistance and to the correlated

[1]Unité Mixte de Physique CNRS/Thales, 1 Avenue Augustin Fresnel, Campus de l'Ecole Polytechnique, 91767 Palaiseau, France and Université Paris-Sud, 91405 Orsay, France, [2]Université d'Evry-Val d'Essonne, Bd. F. Mitterrand, 91025 Evry cedex, France, [3]Department of Materials Science, University of Cambridge, Cambridge CB2 3QZ, UK, [4]Thales Research and Technology, 1 Av. A. Fresnel, Campus de l'Ecole Polytechnique, 91767 Palaiseau, France, [5]National Institute of Advanced Industrial Science and Technology (AIST), Tsukuba, Ibaraki 305-8562, Japan.
*e-mail: agnes.barthelemy@thalesgroup.com.

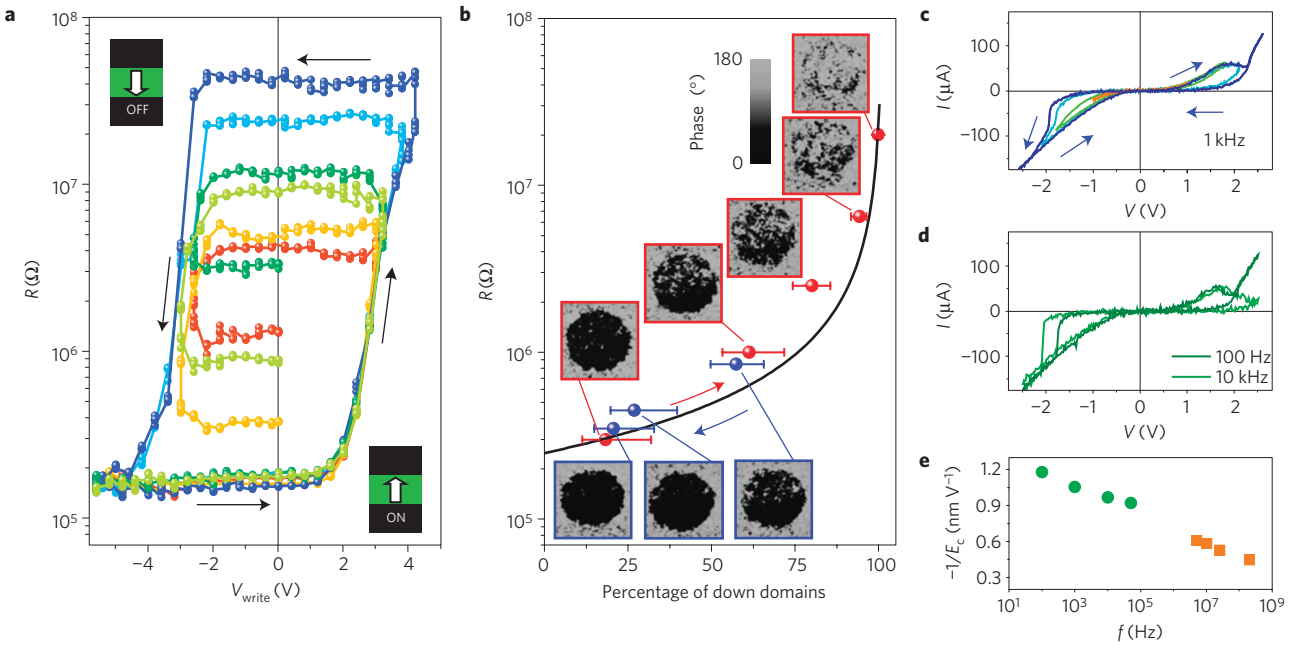

Figure 1 | Tuning resistance and ferroelectric domain configuration with voltage amplitude. a, Dependence of the junction resistance measured at $V_{read} = 100$ mV after the application of 20 ns voltage pulses (V_{write}) of different amplitudes. The different curves correspond to different consecutive measurements, with varying maximum (positive or negative) V_{write}. **b**, Variation of a similar capacitor resistance with the relative fraction of down domains extracted from the PFM phase images. Red-(and blue-)framed images show states achieved by the application of positive (and negative) voltage pulses of increasing amplitude starting from the ON (and OFF) state. The blue and red symbols correspond to the experimental resistance value as a function of the fraction of down domains extracted from the PFM phase images; the black curve is a simulation in a parallel resistance model. The error bars are calculated from the distribution of clear and dark contrasts in the grey level histograms. **c**,**d**, Current versus voltage curves, measured at 1 kHz on a similar capacitor, for various amplitudes of the maximum voltage (**c**) and current versus voltage curves, measured at different frequencies: 100 Hz and 10 kHz (**d**). **e**, Evolution of the inverse of the negative switching field as a function of the measurement frequency. The green circles are extracted from **c**,**d**, and the orange squares from $R(V)$ curves similar to **a** at different pulse durations.

nucleation and propagation of up domains (dark contrast in the blue-framed images).

Overall, the junction resistance shows a systematic variation with the relative fraction of down domains extracted from the PFM images (red and blue symbols in Fig. 1b). This variation can be well reproduced in a simple model (black curve in Fig. 1b) considering that up- and down-polarized regions with different specific resistance conduct current in parallel. Thus, in FTJs, a memristive behaviour can be devised by controlling the nucleation and growth of ferroelectric domains.

The memristive behaviour of the junctions is further confirmed by the current versus voltage curves presented in Fig. 1c,d. As expected[25], the observed pinched-IV loops, characteristics of memristors, expand as the maximum voltage increases (Fig. 1c). Figure 1d shows the IV curves at different frequencies. The inverse switching field scales exponentially with the frequency over seven orders of magnitude (see Fig. 1e), in agreement with recent experiments[26], and conforms to Merz's law.

The junction resistance not only depends on the pulses amplitude but also on their duration and repetition number. Figure 2 presents phase diagrams of the resistance versus pulse duration (in the 10–200 ns range) and pulse number for three different pulse amplitudes. Along with the bipolar switching behaviour, this possibility to vary the resistance through the application of pulse sequences enables a simple scheme to continuously decrease or increase the junction resistance. We applied consecutive trains of positive and negative pulses (Fig. 3) after poling the junction in the ON state (reset). In Fig. 3a,b, we fixed the number of consecutive positive pulses to 10 (amplitude: +2.9 V), which reproducibly set the junction into an intermediate resistance level of 4×10^6 Ω. Clearly, the number of negative pulses (−2.7 V) applied subsequently determines the resistance level of the final state. In Fig. 3c,d, we varied the number of consecutive positive pulses (+3 V) and fixed the number of negative ones (−3 V). The resistance gradually increases with the number of positive pulses, confirming the cumulative effects seen in Fig. 2. Besides, the resistance after each negative pulses sequence depends on the level reached after the previous positive pulse train. Resistance switching from OFF to ON always seems more abrupt than from ON to OFF, which correlates with the asymmetry of the resistance versus voltage cycle in Fig. 1a.

Overall, the results shown in Fig. 3 demonstrate that the resistance level of the FTJ can not only be set by one pulse of appropriate amplitude but also by an appropriate number of consecutive pulses of a fixed voltage. This matches the definition of memristive devices and this latter functionality is particularly appealing for the integration of FTJs in brain-inspired computational architectures. In the particular case of artificial synapses, this would allow the modification of synaptic transmission through spike-timing-dependent plasticity, that is depending on the respective timing of spikes emitted by the pre and post neurons[4,27].

We now analyse the dynamics of resistance switching from ON to OFF and from OFF to ON. Assuming conduction in parallel for regions with $P_\downarrow$ or $P_\uparrow$, we define the relative fraction of down domains by $s = (1/R - 1/R_{ON})/(1/R_{OFF} - 1/R_{ON})$; thus, s varies from 0 in the ON state ($P_\uparrow$) to 1 in the OFF state ($P_\downarrow$). Figure 4 shows a typical set of data on the evolution of s as a function of cumulative pulse time for pulse durations of 10 ns. For positive (negative) pulses, the initial state was initialized to R_{ON} (R_{OFF}) corresponding to $P_\uparrow$ ($P_\downarrow$). Whereas the polarization reversal starts immediately after the first pulse for up-to-down switching (Fig. 4d–f), it is delayed in the down-to-up case with a delay time that depends on the applied voltage (Fig. 4a–c). For both switching directions, s does not

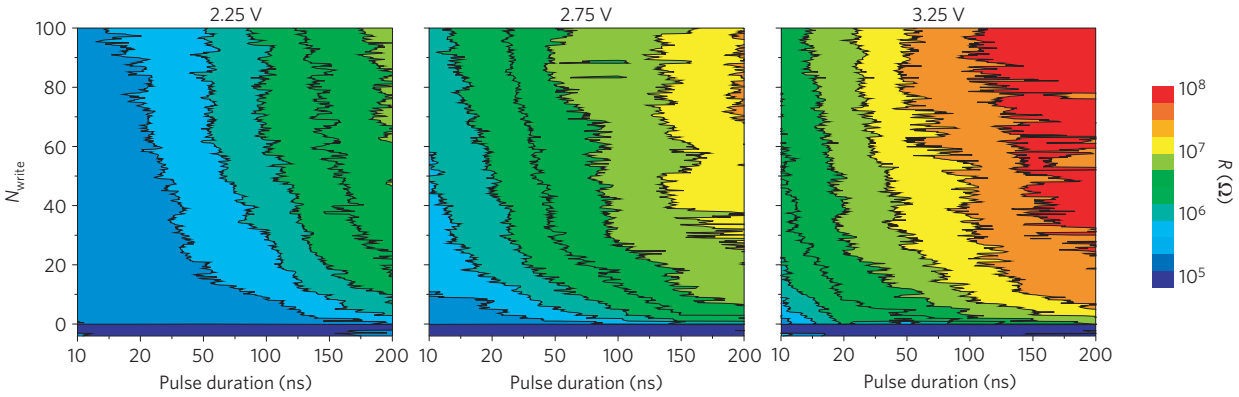

Figure 2 | Experimental pulse duration/pulse number phase diagrams. Resistance of a junction for different pulse durations repeated N_{write} times for three pulse amplitudes.

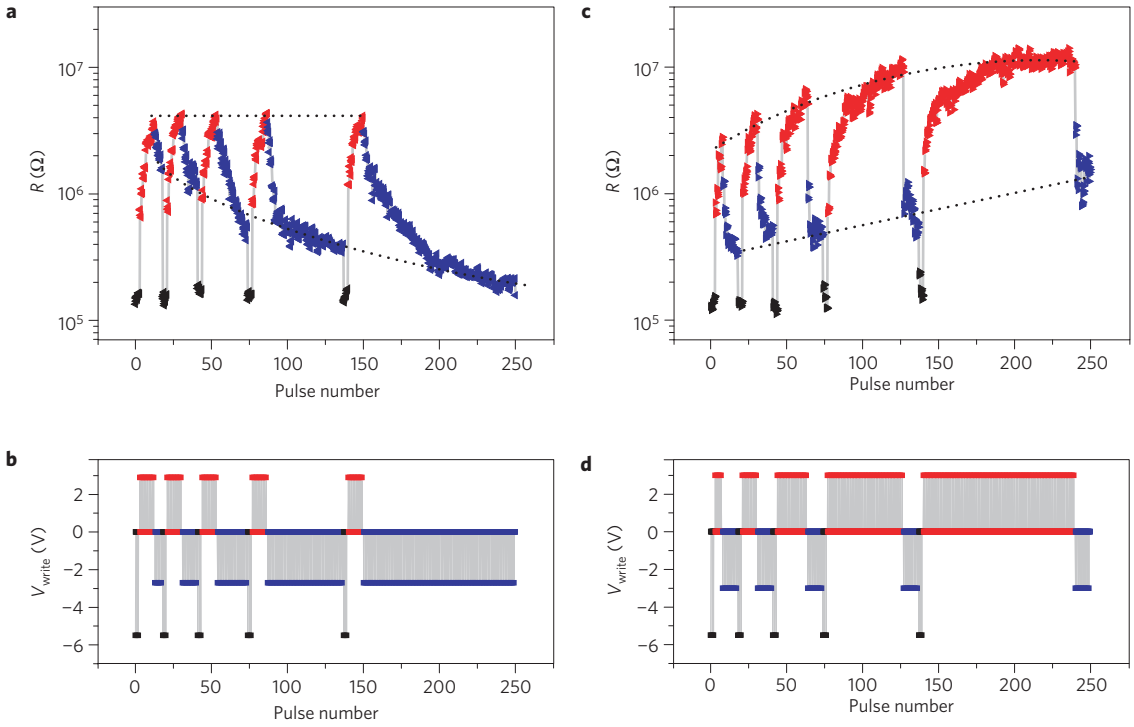

Figure 3 | Tuning resistance by consecutive identical pulses. a–d, Evolution of the junction resistance (**a**,**c**) as a function of the different voltage pulse sequences (**b**,**d**) (plotted for $V_{write} = +2.9$ V and -2.7 V (**a**,**b**) and for $V_{write} = +3$ V and -3 V (**c**,**d**)).

always evolve smoothly towards the final state but presents a more wavy dependence. This signals the presence of several areas with different switching dynamics. This could be due to the submicrometre lithographic process we use to define FTJs, which may introduce a slight polarization disorder, consistent with a previous report[24].

Two main models have been developed to describe the physics of ferroelectric polarization reversal by nucleation and propagation of domain walls. The Kolmogorov–Avrami–Ishibashi (KAI) model[11,12] applies to systems where switching is mainly driven by propagation, which is typically the case for clean epitaxial systems[28]. On the contrary, the nucleation-limited-switching models[29,30] have been developed to describe the dynamics of systems where switching is dominated by nucleation effects in disordered systems[31]. The delayed onset of switching at negative voltage can be ascribed to asymmetric nucleation processes: for up-to-down switching, pinned domains with down polarization serve as pre-existing nucleation centres; on the contrary, for down-to-up switching, nucleation centres need to be activated, explaining the observed delays in the s versus time data (Fig. 4a–c) corresponding to increased nucleation times. We argue that the remainder of the switching process occurs in the propagation regime. This picture discards an interpretation in terms of a purely nucleation-limited scenario.

To account for the observed wavy behaviour we model the data by dividing the pad area into a finite number of zones with different propagation and nucleation kinetics (different domain wall propagation speeds, nucleation times, numbers of nuclei), each ruled by the KAI model. For a given zone i, we suppose that all nucleation sites are activated at the same nucleation time τ_N^i and then propagate with a characteristic propagation time τ_P^i that both depend on the voltage. Following this set of assumptions, the fraction of switched domains s can be written as

$$s = \sum_{i=1}^{N(i)} S_i * h(t-\tau_N^i) * \left\{1 - \exp\left[-\left(\frac{t-\tau_N^i}{\tau_P^i}\right)^2\right]\right\} \qquad (1)$$

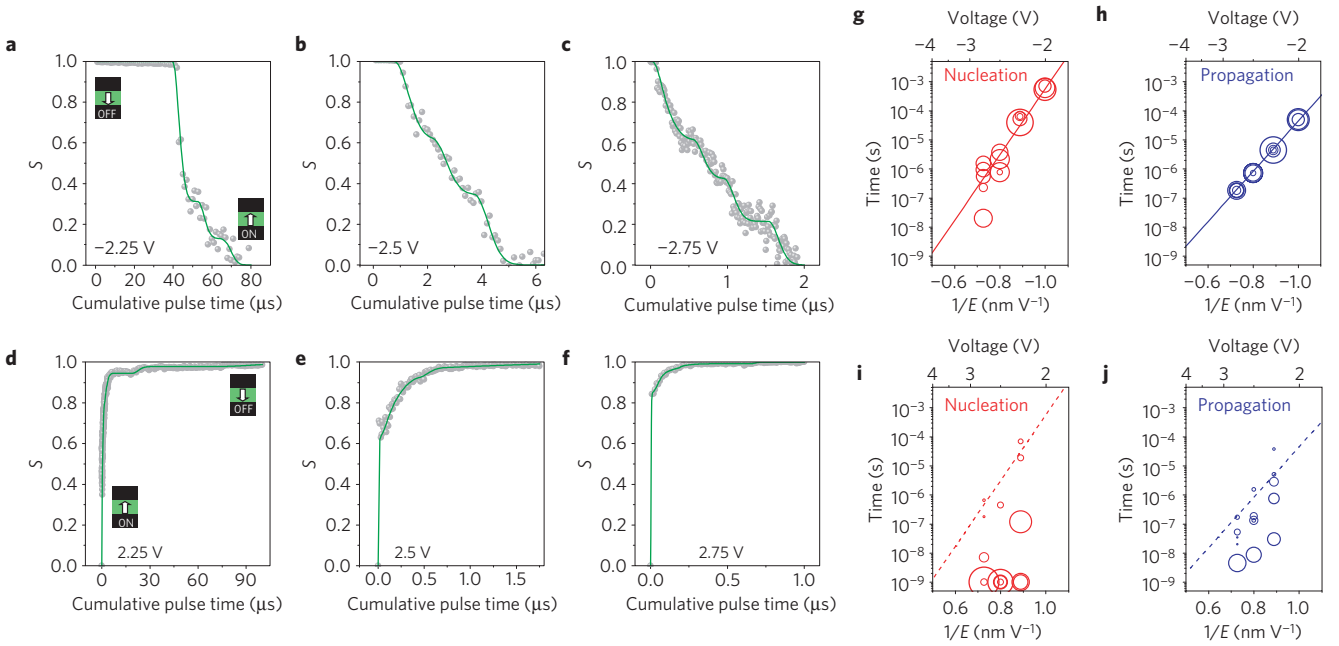

Figure 4 | Polarization switching dynamics. a–f, Dependence of the switched fraction on the cumulative pulse time for down-to-up (**a–c**) and up-to-down (**d–f**) switching and different voltage amplitudes. The data are shown as symbols and the lines are fits (see text for details). **g–j**, Nucleation and propagation times of the different zones, extracted from the fits of the data in **a–f**, plotted as a function of the inverse of the applied electric field, for negative (**g**,**h**) and positive (**i**,**j**) bias. The symbol size is proportional to the corresponding size of the considered zone. The solid lines in **g** and **h** are fits to the time versus $1/E$ data. These lines are replotted as dashed lines in **i** and **j**, respectively.

for up-to-down switching and as

$$s = 1 - \sum_{i=1}^{N(i)} S_i * h(t - \tau_N^i) * \left\{ 1 - \exp\left[-\left(\frac{t - \tau_N^i}{\tau_P^i} \right)^2 \right] \right\} \qquad (2)$$

for down-to-up switching, where S_i is the area of each zone normalized by the total junction area (with $\sum_{i=1}^{N(i)} S_i = 1$) and $h(t)$ is the Heaviside step function.

Figure 4a–c (4d–f) also shows the fit of the experimental data by equation (2) (equation (1)) for negative (respectively, positive) applied voltage with amplitude 2.25, 2.5 and 2.75 V. The data are well fitted on the whole time range; in particular the wavy dependence of s versus time is accurately reproduced with a reduced number of zones $N \leq 5$. From the fits, we can extract for each zone the nucleation and propagation times that are plotted as a function of electric field for negative (Fig. 4g,h) and positive bias (Fig. 4i,j). The size of each symbol is proportional to the area S_i of the zone it represents.

Both nucleation and domain wall propagation follow Merz's law, being proportional to $\exp(-E_a/E)$ (refs 26,31; see Fig. 4g,h and the Supplementary Information for a more detailed discussion). The activation fields for nucleation $E_a(\mathrm{N})$ and propagation $E_a(\mathrm{P})$ are of the same order of magnitude, respectively 2.6×10^{10} and 2.0×10^{10} V m^{-1}. Reported values for the activation fields are quite variable in the literature, ranging from 4×10^5 V m^{-1} in the bulk to about 2×10^8 V m^{-1} for nanocapacitors with dimensions similar to our pads, but with a film thickness of 35 nm (ref. 26). The larger values we find here may be due to the highly strained character of our ultrathin ferroelectric films, in agreement with the large measured coercive fields[14,32].

Importantly, the quantitative agreement between our model and the experimental data provides us with an analytical expression accounting for the observed memristive response based on the physical description of the ferroelectric domain dynamics. The memory effect typical of memristive systems can be defined by the following two equations[25]:

$$V(t) = R(\sigma, V, i) i(t) \qquad (3)$$

$$\mathrm{d}\sigma/\mathrm{d}t = f(\sigma, V, t) \qquad (4)$$

where σ represents one or several state variables, V is the voltage, i is the current, t is the time and R and f are system-dependent functions. The nonlinear resistance R depends on V, t and σ that varies over time as described in equation (4). Equations (3) and (4) impose a strict framework for resistive switching devices to truly behave as memristive systems. One of the first implications of this definition is that the resistance should vary continuously with V.

In the case of FTJs, we propose that the volume fraction of down domains can be used as the state variable; that is, we identify s with σ. Then, in the simple case of switching by a single zone (a situation that might be achievable in fully patterned, fully epitaxial FTJs), we can write

$$\mathrm{d}s/\mathrm{d}t = (1 - s) \times \left\{ \frac{2}{\tau_\mathrm{P}(V)} \left(\frac{t - \tau_\mathrm{N}(V)}{\tau_\mathrm{P}(V)} \right) \right\} = f(s, V, t) \qquad (5)$$

In contrast to the situation for most other existing memristive systems, we thus reach a description of ferroelectric memristors that goes beyond basic phenomenology and we provide the expression of the function f in equation (4) for the temporal evolution of the state parameter based on physical arguments.

We have reported transport measurements in ferroelectric tunnel junctions as a function of the amplitude, duration and number of voltage pulses. The resistance can be continuously and reversibly tuned over more than two orders of magnitude by varying the pulse amplitude and/or the pulse number (and thus the total integrated excitation time). These features qualify FTJs as memristive devices. This improves on previous memristors with a purely electronic mechanism where the resistance contrast is no better than a factor of two[6,7]. Relying on the correlation

between junction resistance and ferroelectric domain structure (as imaged by PFM), we model the resistive switching behaviour using a simple model of domain nucleation and growth in a heterogeneous medium. We derive an analytical expression ruling the memristive response, which exemplifies the advantage of resorting to well-established physical phenomena such as ferroelectricity in the design of memristive systems. Our results invite further investigations of switching dynamics in nanoscale ferroelectrics and open unforeseen perspectives for ferroelectrics in next-generation neuromorphic computational architectures.

Methods

Samples. The BTO/LSMO bilayers were grown on (001)$NdGaO_3$ single-crystal substrates by pulsed laser deposition (KrF excimer laser ($\lambda = 248$ nm), fluence of 2 J cm^{-2}, repetition rate of 1 Hz). LSMO films of 30 nm in thickness were grown at 775 °C under 0.15 mbar of oxygen pressure. BTO films were subsequently grown at 775 °C and 0.10 mbar oxygen pressure. The samples were annealed for 1 h at 750 °C and 500 mbar oxygen pressure and cooled down to room temperature at 10°C min^{-1}. The thickness of the films was calibrated with X-ray reflectivity and cross-checked with transmission electron microscopy. The nanodevices with diameters of 350 nm were defined from these bilayers by electron-beam lithography and lift-off of sputter-deposited Co (10 nm) followed by a capping layer of Au (10 nm).

Measurements. Electrical measurements were performed with a Digital Instruments Nanoscope IV set-up at room temperature and under nitrogen flow with commercial Si tips coated with Cr/Pt (Budget Sensors). The bias voltage was applied to the tip and the sample was grounded for electrical measurements. For voltage pulse time widths below 500 ns, a bias tee was connected to the atomic force microscope to split voltage pulses from d.c. measurements. An Agilent 81150A pulse generator was used to apply voltage pulses of duration of 10–200 ns and resistances after the applied pulses were measured with a Keithley 6487 picoammeter using a Yokogawa GS610 voltage source at 100 mV.

PFM experiments were performed with a multimode Nanoscope IV set-up and SR830 lock-in detection. A TTi TG1010 external source was used to apply a 12 kHz a.c. sinusoidal excitation of 1 V peak to peak with a d.c. offset of 100 mV. The tip was grounded for PFM experiments. Successive PFM images were collected after setting the device to a chosen resistance state by application of 100 µs voltage pulses.

Switching dynamics model. The model is based on the following assumptions: the switching occurs through zones with different parameters in terms of domain wall propagation speed, nucleation time and number of nuclei; each zone follows the KAI model; for a given zone, we suppose that all nucleation sites are activated at the same time $t = \tau_N$, the nucleation time. τ_N depends on the voltage. The number of zones involved in the switching process may depend on the voltage.

Following this set of assumptions, the ratio s can be written as

$$s = \sum_{i=1}^{N(i)} S_i * h(t - \tau_N^i) * \left\{ 1 - \exp\left[-\left(\frac{t - \tau_N^i}{\tau_P^i} \right)^2 \right] \right\}$$

for up-to-down switching, and

$$s = 1 - \sum_{i=1}^{N(i)} S_i * h(t - \tau_N^i) * \left\{ 1 - \exp\left[-\left(\frac{t - \tau_N^i}{\tau_P^i} \right)^2 \right] \right\}$$

for down-to-up switching with $\sum_{i=1}^{N(i)} S_i = 1$.

Received 17 May 2012; accepted 31 July 2012; published online 16 September 2012

References

1. Chua, L. O. Memristor—the missing circuit element. *IEEE Trans. Circuit Theory* **18,** 507–519 (1971).
2. Strukov, D. B., Snider, G. S., Stewart, D. R. & Williams, R. S. The missing memristor found. *Nature* **453,** 80–83 (2008).
3. Yang, J. J. *et al.* Memristive switching mechanisms for metal/oxide/metal nanodevices. *Nature Nanotech.* **3,** 429–433 (2008).
4. Jo, S. H., Chang, T., Bhadviya, B. B., Mazumder, P. & Lu, W. Nanoscale memristor device as synapse in neuromorphic systems. *Nano Lett.* **10,** 1297–1301 (2010).
5. Kwon, D-H. *et al.* Atomic structure of conducting nanofilaments in TiO_2 resistive switching memory. *Nature Nanotech.* **5,** 148–153 (2010).
6. Wang, X., Chen, Y., Xi, H., Li, H. & Dimitrov, D. Spintronic memristor through spin-torque-induced magnetization motion. *IEEE Electron Device Lett.* **30,** 294–297 (2009).
7. Chanthbouala, A. *et al.* Vertical-current-induced domain-wall motion in MgO-based magnetic tunnel junctions with low current densities. *Nature Phys.* **7,** 626–630 (2011).
8. Esaki, L., Laibowitz, R. B. & Stiles, P. J. Polar switch. *IBM Tech. Discl. Bull.* **13,** 2161 (1971).
9. Garcia, V. *et al.* Giant tunnel electroresistance for non-destructive readout of ferroelectric states. *Nature* **460,** 81–84 (2009).
10. Bibes, M., Grollier, J., Barthélémy, A. & Mage, J-C. Ferroelectric device with adjustable resistance, WO 2010142762 A1 (2010).
11. Ishibashi, Y. & Takagi, Y. Note on ferroelectric domain switching. *J. Phys. Soc. Jpn* **31,** 506–510 (1970).
12. Orihara, H., Hashimoto, S. & Ishibashi, Y. Study on D–E hysteresis loop of TGS based on the Avrami-type model. *J. Phys. Soc. Jpn* **63,** 1601–1610 (1994).
13. Gruverman, A. *et al.* Tunneling electroresistance effect in ferroelectric tunnel junctions at the nanoscale. *Nano Lett.* **9,** 3539–3543 (2009).
14. Chanthbouala, A *et al.* Solid-state memories using ferroelectric tunnel junctions. *Nature Nanotech.* **7,** 101–104 (2012).
15. Pantel, D., Goetze, S, Hesse, D & Alexe, M. Room-temperature ferroelectric resistive switching in ultrathin $Pb(Zr_{0.2}Ti_{0.8})O_3$ films. *ACS Nano* **5,** 6032–6038 (2011).
16. Zhuravlev, M. Y., Sabirianov, R. F., Jaswal, S. S. & Tsymbal, E. Y. Giant electroresistance in ferroelectric tunnel junctions. *Phys. Rev. Lett.* **94,** 246802 (2005).
17. Kohlstedt, H., Pertsev, N. A., Rodriguez Contreras, J. & Waser, R. Theoretical current–voltage characteristics of ferroelectric tunnel junctions. *Phys. Rev. B* **72,** 125341 (2005).
18. Tsymbal, E. Y. & Kohlstedt, H. Tunneling across a ferroelectric. *Science* **313,** 181–183 (2006).
19. Catalan, G., Scott, J. F., Schilling, A. & Gregg, J. M. Wall thickness dependence of the scaling law for ferroic stripe domains. *J. Phys. Condens. Matter* **19,** 022201 (2007).
20. Catalan, G. *et al.* Fractal dimension and size scaling of domains in thin films of multiferroic $BiFeO_3$. *Phys. Rev. Lett.* **100,** 027602 (2008).
21. Bibes, M. Nanoferronics is a winning combination. *Nature Mater.* **11,** 354–357 (2012).
22. Bolten, D., Böttger, U. & Waser, R. Effect of interfaces in Monte Carlo computer simulations of ferroelectric materials. *Appl. Phys. Lett.* **84,** 2379–2381 (2004).
23. Kim, D. J. *et al.* Observation of inhomogeneous domain nucleation in epitaxial $Pb(Zr, Ti)O_3$ capacitors. *Appl. Phys. Lett.* **91,** 132903 (2007).
24. Gruverman, A. Wu & Scott, J. F. Piezoresponse force microscopy studies of switching behavior of ferroelectric capacitors on a 100-ns time scale. *Phys. Rev. Lett.* **100,** 097601 (2008).
25. Chua, L. O. & Kang, S. M. Memristive devices and systems. *Proc. IEEE* **64,** 209–223 (1976).
26. Shin, Y-H., Grinberg, I., Chen, I-W. & Rappe, A.M. Nucleation and growth mechanism of ferroelectric domain-wall motion. *Nature* **449,** 881–884 (2007).
27. Linares-Barranco, B. & Serrano-Gotarredona, T. Memristance can explain spike-time-dependent-plasticity in neural synapses, Available from *Nature Precedings* http://hdl.handle.net/10101/npre.2009.3010.1 (2009).
28. Jo, J. Y. *et al.* Nonlinear dynamics of domain-wall propagation in epitaxial ferroelectric thin films. *Phys. Rev. Lett.* **102,** 045701 (2009).
29. Du, X. F. & Chen, I. W. Fatigue of $Pb(Zr_{0.53}Ti_{0.47})O_3$ ferroelectric thin films. *J. Appl. Phys.* **83,** 7789–7798 (1998).
30. Tarangtsev, A. K., Stolichnov, I., Setter, N., Cross, J. S. & Tsukada, M. Non-Kolmogorov–Avrami switching kinetics in ferroelectric thin films. *Phys. Rev. B* **66,** 214109 (2002).
31. Jo, J. Y. *et al.* Domain switching kinetics in disordered ferroelectric thin films. *Phys. Rev. Lett.* **99,** 267602 (2007).
32. Pertsev, N.A. *et al.* Coercive field of ultrathin $Pb(Zr_{0.52}Ti_{0.48})O_3$ epitaxial films. *Appl. Phys. Lett.* **83,** 3356–3358 (2003).

Acknowledgements

Financial support from the European Research Council (ERC Advanced Grant No. 267579 and ERC Starting Grant No. 259068) and the French Agence Nationale de la Recherche (ANR) MHANN and NOMILOPS are acknowledged. X.M. acknowledges Herchel Smith Fellowship support. We would like to thank J. F. Scott, B. Dkhil and L. Bellaiche for useful comments.

Author contributions

V.G., M.B., A.B. and J.G. designed the experiment. X.M., S.X., H.Y., C.D. and N.D.M. fabricated the samples. A.C., V.G., K.B., S.F. and M.B. performed the measurements. A.C., V.G., R.O.C., M.B., A.B. and J.G. analysed the data. M.B., A.B. and J.G. wrote the manuscript. All authors discussed the data and contributed to the manuscript.

Additional information

Supplementary information is available in the online version of the paper. Reprints and permissions information is available online at www.nature.com/reprints. Correspondence and requests for materials should be addressed to A.B.

Competing financial interests

The authors declare no competing financial interests.